



OPEN SBK3 suppresses angiotensin II-induced cardiac hypertrophy by regulating mitochondrial metabolism

Aihua Yang, Jiabin Cao, Jiaona Gu, Xiaofang Zhu, Yi Qian, Hongyan Qian, Wenjing Zhao, Yuhang Wang & Weizhong Zhu✉

Pathological cardiac hypertrophy is one of the risk factors for heart failure, characterized by elevated levels of renin-angiotensin II (Ang II) and catecholamines. SBK3 (SH3 domain binding kinase family member 3), a resident protein in the mitochondria, exhibits relatively high expression selectively in cardiac tissue based on human protein atlas database. Here, we studied the role of SBK3 in Ang II-induced cardiac hypertrophy to identify a new treatment for cardiac hypertrophy and heart failure by targeting mitochondria. The present study, for the first time, reveals the mitochondrial localization of SBK3 in rat cardiomyocytes and demonstrates a decrease in SBK3 protein expression in angiotensin II-perfused mice hearts. We found that maintaining high levels of SBK3 expression both *in vivo* and *in vitro* significantly suppressed Ang II-induced cardiac hypertrophy. This is attributed to the fact that overexpression of SBK3 rebalanced the levels of oxidative stress and energy metabolism induced by angiotensin II and inhibited the phosphorylation of dynamin-related protein 1 (Drp1) at the serine 616 site (S616) in cardiomyocytes and mice hearts. These findings suggest that SBK3 is a newly discovered mitochondrial protein capable of suppressing cardiac hypertrophy.

Keywords SBK3, Drp1, Hypertrophy, Mitochondria, Heart

Pathological cardiac hypertrophy caused by activation of neurohormone activation is considered to be one of the independent risk factor for heart failure^{1,2}, which is an increasingly serious public health problem. Neurohormone blockers (including adrenergic receptor blockers, angiotensin-converting enzyme inhibitors, and angiotensin II (Ang II) receptor AT1 blockers) are commonly used to treat pathological hypertrophy and heart failure in the clinic^{3–5}. However, the survival rate of patients with heart failure is still low⁶. Changes in mitochondrial function are closely related to cardiac hypertrophy and heart failure⁷. Cell and whole animal model studies have consistently shown that the mitochondrial structure, function and metabolism of hypertrophic hearts are altered^{8–10}. Compensatory cardiac hypertrophy is related to the relative preservation of mitochondrial function^{7,11,12}. The imbalance between mitochondrial bioenergetics and the cardiac hypertrophy phenotype is crucial to the progression from pathologic myocardial hypertrophy to heart failure. This disparity in pace plays a key role in driving the transition towards heart failure¹³. Therefore, allowing mitochondria to reverse hypertrophy in cardiomyocytes and maintain mitochondrial function is a promising therapeutic method for preventing cardiac hypertrophy or slowing down the transition from cardiac hypertrophy to heart failure.

SH3 domain binding kinase family member 3 (SBK3), also known as SGK110, is encoded by DNA on human chromosome 19¹⁴. The SH3 domain binding kinase (SBK) family comprises SBK1, SBK2 and SBK3. SBK1 is a widely expressed cytoplasmic protein with carcinogenic potential, playing a crucial role in the progression of various tumors^{15–18}. Limited information is available regarding the functions of SBK2 and SBK3. In 2022, Pim R van Gorp et al. first reported that SBK2 is a newly discovered gene enriched in atrial tissue that can regulate sarcomere integrity. The closest relative to SBK2 is SBK3, located only a few kb apart from each other, highlighting their common origin¹⁹. According to the analysis of RNA abundance in Human Protein Atlas (HPA) database, SBK3 is distributed mainly in the heart, tongue, skeletal muscle and adipose tissue. The mRNA abundance of SBK3 in the heart is approximately 78 times higher than that in the lungs and kidneys, 100 times higher than that in the stomach, and 300 times higher than that in the liver. A genome-wide association study (GWAS) confirmed the expression specificity of SBK3 in cardiac tissue and also revealed its close association with cardiovascular

Department of Pharmacology, School of Medicine and School of Pharmacy, Nantong University, Nantong 226001, China. ✉email: Zhuwz@ntu.edu.cn

and metabolic¹⁴. However, there have been no reports thus far on its regulatory activity, cell distribution, and functions in cardiomyocytes and the heart. In this study, the expression of SBK3 was manipulated through gene transfection in rat cardiomyocytes *in vitro* and mouse hearts *in vivo* to investigate the role of SBK3 in Ang II-induced cardiac hypertrophy and its underlying molecular mechanism.

Materials and methods

Reagents and materials

Angiotensin II was obtained from MCE (Shanghai, China). Medium 199, type II collagenase, and protease type XIV were provided by SigmaAldrich (St. Louis, MO, USA). Laminin was obtained from Roche (Basel, Switzerland). Trypsin–EDTA solution, ATP assay kit, lipid peroxidation MDA assay kit (MDA), total superoxide dismutase assay Kit, Cu/Zn-SOD and Mn-SOD assay Kit, cell mitochondria isolation Kit and protein assay kit were obtained from Beyotime (Shanghai, China). FITC Phalloidin was provided by Yeasen Biotechnology (Shanghai, China). MitoSOX Red and Pierce Classic IP Kit were obtained from ThermoFisher (Waltham, MA, USA). Oxygen consumption assay kit was from Best Bio (Shanghai, China). Anti-SBK3 (PA5-48684, PA5-85058) was obtained from ThermoFisher (Waltham, MA, USA). Total OXPHOS Rodent Cocktail antibody (ab110413) which contains 5 mouse mAbs, the mitochondrial complexes I–V, was obtained from Abcam (Cambridge, UK). Anti-COX IV (#4844), anti-Drp1 (#8570), Phospho-Drp1 (#3455), anti-Mitofusin-1 (#14739), Anti-Mitofusin-2 (#9482), anti-OPA1 (#80471) were purchased from Cell Signaling Technology (Danvers, MA, USA). Anti- β -Tubulin (66240-1-Ig), anti-Flag (20543-1-AP) were purchased from Proteintech (Wuhan, China). Hematoxylin–eosin (HE), Masson's trichrome staining kits, and electron microscope fixation solution were obtained from Servicebio (Wuhan, China).

Construction of viruses

All of the viruses used in the experiment were purchased from Jikai (Shanghai, China). The adenovirus vectors were engineered to facilitate the overexpression of SBK3 *in vitro*. The structural framework was mCMV-SBK3-3Flag-SV40-EGFP for one vector. To avoid the interference caused by green fluorescence, another structural framework was designed as mCMV-SBK3-3Flag (AD-SBK3). The adeno-associated virus vector 9 containing mice SBK3, driven by the cardiomyocyte-specific promoter cTNT, were used to ensure specific expression in heart tissue. The structural framework was AAV9-cTNT-SBK3-flag-GFP (AAV9-SBK3).

Animals and treatment

All experimental procedures in animal research conformed to the guidelines for laboratory animal care and were approved by the Ethics Committee for Animal Experiments of Nantong University (approval number IACUC20210916-1001). Studies involving animals were conducted in accordance with the recommendations in the ARRIVE guidelines. C57BL/6 mice, neonatal (1–3 days) and adult Sprague–Dawley (SD) rats were purchased from Animal Centre of Nantong University. Neonatal rats and adult SD rats were utilized for the preparation of cardiomyocytes. C57BL/6 mice were given sterilized water or Ang II (1000 ng/kg/min)²⁰. The mice were positioned on a heated platform at 37°C. Then animals were lightly anaesthetized with 1.5–2% isoflurane. Following this, micro-osmotic pumps (Alzet, USA) were subcutaneously implanted into the dorsal region. Echocardiography of mice was performed under the same anesthetic protocol. Long-axis M-mode images were acquired with a maintained heart rate of 400–500 beats per minute. Usually, at the end, the mice were euthanized with CO₂ gas. Specifically, the mice were placed in a sealed container, and then carbon dioxide gas was introduced to gradually increase the concentration of carbon dioxide in the container, resulting in the rat suffering from hypoxia, being anesthetized, and eventually dying. Once the mouse stopped breathing, the chest was immediately opened to remove the heart, and carry out other necessary experimental operations as described in the method section.

Histological analysis

The mice were anaesthetized by intraperitoneal injection of 0.5% pentobarbital sodium (0.1 ml/10 g). Left ventricular specimens were fixed with 4% paraformaldehyde and embedded in paraffin. Cardiac sections were analyzed by histology and immunohistochemistry to determine cardiomyocyte hypertrophy and fibrosis. Haematoxylin/eosin (HE)²¹ and Masson trichrome staining (Masson) were used to evaluate the degree of cardiac fibrosis, and wheat germ agglutinin (WGA) was used to evaluate the cross-sectional area of the cardiomyocytes.

Transmission electron microscope

The 1 mm³ mouse heart tissue was immediately placed in a petri dish containing electron microscope fixation solution. It was then fixed at room temperature for 2 h, transferred to an EP tube, and further fixed at 4 °C. After gradient dehydration, the sample was permeated and polymerized overnight. Subsequently, an ultrathin film of 60–80 nm was cut and double-stained with 2% uranyl acetate and 2.6% lead citrate. Following drying, the images were observed and collected using a transmission electron microscope.

Serum biochemistry analysis

Lactate dehydrogenase (LDH) and creatine kinase (CK) levels in serum samples were determined with kits according to the manufacturer's instructions (Jiancheng Ltd., Nanjing, China).

Isolated and cultured rat cardiomyocytes

The adult rat cardiomyocytes (ARCMs)²¹ and neonatal rat cardiomyocytes (NRCMs)²² used in the experiment were isolated and cultured by enzymatic hydrolysis as previously described. ARCMs were prepared from hearts of adult (220–250 g) SD rats. NRCMs were prepared from hearts of neonatal rats born for 1–3 days. ARCMs were

cultured in M199 medium, while NRCMs were cultured in DMEM/F-12 medium. The cardiomyocytes were transfected with adenovirus, which was dissolved in the enhancing solution, for 8 h, after which the medium was replaced with fresh medium as described above. Due to differences in cell viability, ARCMs were cultured for 60 h for total. NRCMs were cultured for 72 h for total.

Immunofluorescence

The cells were washed. After immunostaining fixing, permeabilization and blocking for 10 min respectively, the primary antibody was added and incubated overnight at 4 °C. The primary antibody was discarded, and the secondary antibody was added and incubated at room temperature for 2 h. After DAPI stained the nucleus, it was sealed with fluorescence quencher and observed under confocal microscope. The MitoTracker dye was employed for mitochondrial localization when necessary²³.

Phalloidin staining

After fixation and permeabilization, preprepared Phalloidin working solution (100 nM) was added in cells, and the mixture was incubated at room temperature for 30 min in the dark. After washing with PBS, Hoechst was added, and the samples were incubated at room temperature for 10 min in the dark. An anti-quench agent was added to seal the cells, and the phalloidin-stained actin filaments were observed and evaluated under a fluorescence microscope.

Analysis of ATP levels and extracellular oxygen consumption

ATP levels in cardiomyocytes were determined via an ATP assay kit. The specific oxygen fluorescent probe BBoxiProbe®R01 was used to detect changes in extracellular oxygen consumption. The proteins were measured directly by a fluorescent enzyme-labelled instrument.

Analyses of oxidative stress indices

MitoSOX™ was used to determine the level of ROS in the mitochondria of live cardiomyocytes. The images were collected by laser confocal microscopy and analysed. Malondialdehyde (MDA), superoxide dismutase (SOD) and Mn-SOD (SOD₂) levels were determined via kit detection or Western blotting.

Co-immunoprecipitation (Co-IP)²³

Adult rat cardiomyocytes were isolated and cultured and inoculated in two large dishes with a diameter of 10 mm, which were divided into AD-SBK3 group and AD-SBK3 + AngII group. AD-SBK3 overexpressed adenovirus was transfected for 60 h. Then follow the instructions in the Pierce Classic IP Kit. Specifically, the treated adherent cells were first eluted with the lysate. Pre-clear lysate using the Control Agarose Resin. Discard the column containing the Control Agarose resin and save the flow-through, which will be added to the corresponding antibody. Incubate overnight at 4 °C to form the immune complex. Next day, add the antibody/lysate sample to Protein A/G Plus Agarose in the spin column. Attach the screw cap and incubate column with gentle end-over-end mixing or shaking for 1 h. Different elution methods were used according to the experimental purpose after pre-washing, for mass spectrographic analysis or Western Blot.

qPCR

Total RNA was extracted using the FastPure Cell/Tissue Total RNA Isolation Kit. Reverse transcription was performed with the PrimeScript™ RT reagent Kit. Then, using GAPDH as an internal reference gene, cDNA was amplified using SYBR Green reagents. Analysis was performed using the 2^{-ΔΔCt} method²⁴. The sequences of all the primers (Sangon Biotech, Shanghai, China) used are listed in Table 1.

Western blotting

Proteins were extracted from isolated heart tissue or rat cardiomyocytes, separated via sodium dodecyl sulfate-polyacrylamide gel electrophoresis (SDS-PAGE) and subsequently blotted onto polyvinylidene difluoride (PVDF) membranes. The entire membranes were cut prior into pieces under the guidance of the Marker with different molecular weights, different primary antibodies were used respectively for an overnight incubation. Next day, the membranes were incubated with the fluorescent secondary antibodies for 2 h at room temperature after primary antibodies discarded. When performing the development, the membrane pieces were still placed together for development according to the molecular weights of the marker. Images were acquired by scanning on a fluorescence developer, which were analyzed by image J.

Genes	Species	Forward primer (5'-3')	Reverse primer (5'-3')
ANP	Rat	GAGAGTGAGCCGAGACAGCAAAC	GGAAGAAGCCCTTGGTGATGGAG
BNP	Rat	AGTCTCCAGAACAATCCACGATGC	GCCTTGGTCTTTGAGAGCTGTCT
GAPDH	Rat	AAATGGTGAAGGTCCGTGTGAAC	CAACAATCTCCACTTTGCCACTG
ANP	Mouse	GAGAAAGATGCCGGTAGAAGA	AAGCACTGCCGTCTCTCAGA
BNP	Mouse	CTGCTGGAGCTGATAAGAGA	TGCCCAAAGCAGCTTGAGAT
SBK3	Mouse	GCGGCTAGTGGAGCTAACAG	AGGGTCTGTAGTAGGCCTGG
GAPDH	Mouse	AGTCCCTGCCCTTTGTACACA	CGATCCGAGGGCCTCACTA

Table 1. Primer sequences used in real-time PCR.

Statistical analysis

The data were presented as mean \pm S.E.M. from three or six independent experiments as described in figure legends. Statistical analyses were performed using GraphPad Prism. The significant differences were analyzed using an independent sample t-test or one-way ANOVA following by Student–Newman–Keuls test. $P < 0.05$ was considered to indicate a statistically significant difference.

Results

The mitochondrial protein SBK3 is downregulated in mice hearts with cardiac hypertrophy

In 8-week-old C57BL/6 wild-type male mice, micro-osmotic pump infused with Ang II (1000 ng/kg/min) was implanted subcutaneously, while sterilized water was used in the control pump. After 14 days, M-mode images are utilized for the detection of ventricular wall thickness and assessment of cardiac function.

The results (Fig. 1A,B) showed that Ang II administration for 2 weeks significantly increased the ventricular septum and left ventricular wall thickness at both end-diastole and end-systole. After all of experimental mice were humanely euthanized, their hearts were collected and weighed, and the ratio of heart weight to body weight (BW/HW) was calculated. Tissue sections were prepared for hematoxylin and eosin (HE) staining as well as Masson staining. The findings indicated that the hearts in AngII-treated mice were significantly larger than in control mice, as evidenced by that BW/HW ratio (Fig. 1C,E) was increased compared to the control group. In addition, AngII stimulation resulted in a disorganized arrangement of myocardial tissue structures, accompanied by a significant increase in Masson staining positive area (Fig. 1C,D). These suggested that Ang II perfusion induced cardiac hypertrophy.

Cardiac proteins from mouse were subsequently extracted for Western blot analysis. The results revealed a significant decrease in SBK3 protein expression in mice following 2 weeks of Ang II perfusion, as compared to

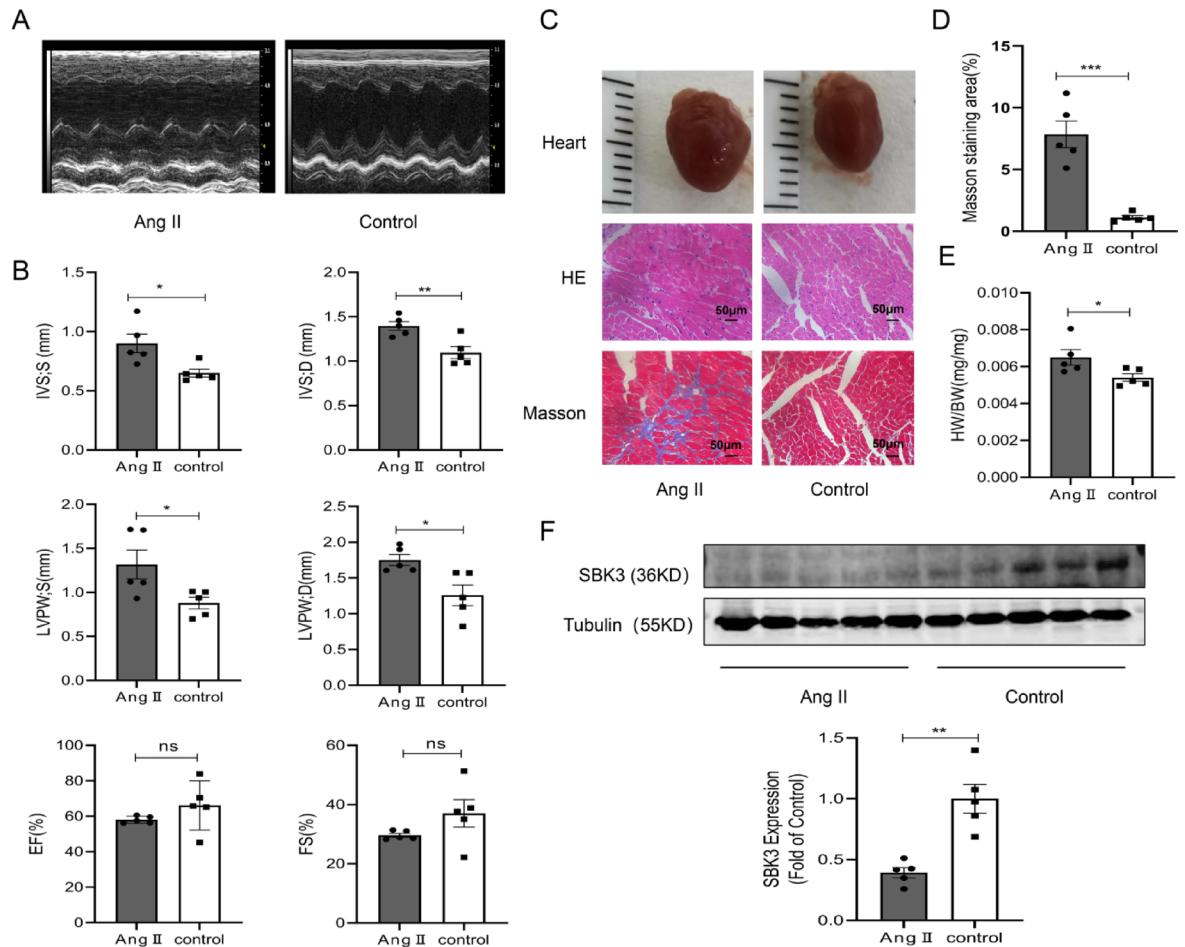


Fig. 1. The expression of SBK 3 protein was reduced in myocardium of mice with hypertrophy induced by Ang II. (A,B) Echocardiography representative images (A) and quantitative analysis (B) in Ang II-perfused and control mice. (C) Representative images of mouse heart, HE and Masson's trichrome staining; Scale bars = 500 μ m. (D) Quantitative analysis of the masson staining. (E) Ratio of heart weight to body weight (HW/BW) in mice. (F) SBK3 protein expression in Ang II and control groups (western blot). $n = 5$ mice per group. The data were expressed as Mean \pm SEM. * $p < 0.05$, ** $p < 0.01$, *** $p < 0.001$ ns, non significant; an independent sample t-test.

control mice (Fig. 1F). This indicated a reduced level of SBK3 protein expression in heart tissue during cardiac hypertrophy.

AAV9-SBK3 suppresses Ang II-induced hypertrophy in mice

To further elucidate effect of SBK3 on cardiac hypertrophy *in vivo*, we constructed an SBK3 adeno-associated virus 9 (AAV9-SBK3) driven by the cardiomyocyte-specific promoter cTNT. Tissue fluorescence (Fig. 2A), Western blot (Fig. 2B) and qPCR (Fig. 2C) analysis confirmed the stable expression of AAV9-SBK3 in mice myocardium. In our experiment, we subcutaneously implanted micro-osmotic pumps containing Ang II (1000 ng/kg/min) or sterile water into mice, AAV9-SBK3 or AAV9-Flag was injected at an optimal dose of 5×10^{11} v.g through the tail vein. The observation period lasted for six weeks. Firstly, echocardiography (Fig. 3A,B) revealed that overexpression of SBK3 alone had no significant effect on physiological structure or cardiac function. Although Ang II had no effect on the ejection fraction (EF), fractional shortening (FS), it significantly increased the thickness of the interventricular septum (IVS) and left ventricular posterior wall (LVPW) in mice. These findings indicated the successful induction of cardiac hypertrophy in mice. More importantly, AAV9-SBK3 effectively inhibited the Ang II-induced increase in IVS and LVPW thickness.

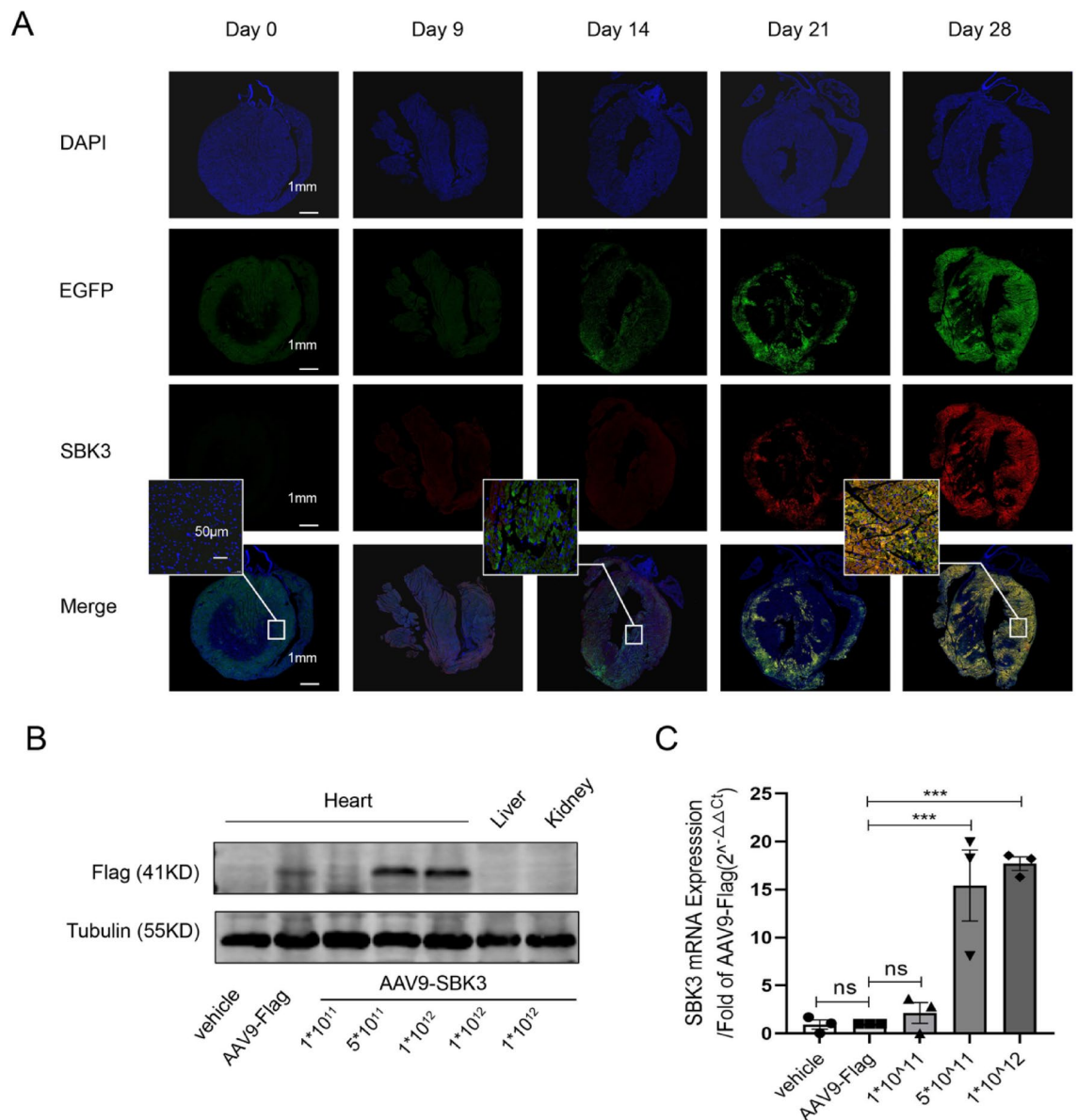


Fig. 2. SBK3 was successfully overexpressed in the hearts of mice. (A–C) AAV9-SBK3 were successfully expressed in mice heart determined by immunofluorescence (A, scale bar = 1000 μ m), Western blotting (B) and qPCR (C, n = 3). On the 28th day post-infection, proteins and mRNA were extracted from heart tissue, and the expression of SBK3 was subsequently assessed. The data were expressed as Mean \pm SEM. $^{**}P < 0.01$, ns, non significant; one-way ANOVA test, followed by the Newman–Keuls test.

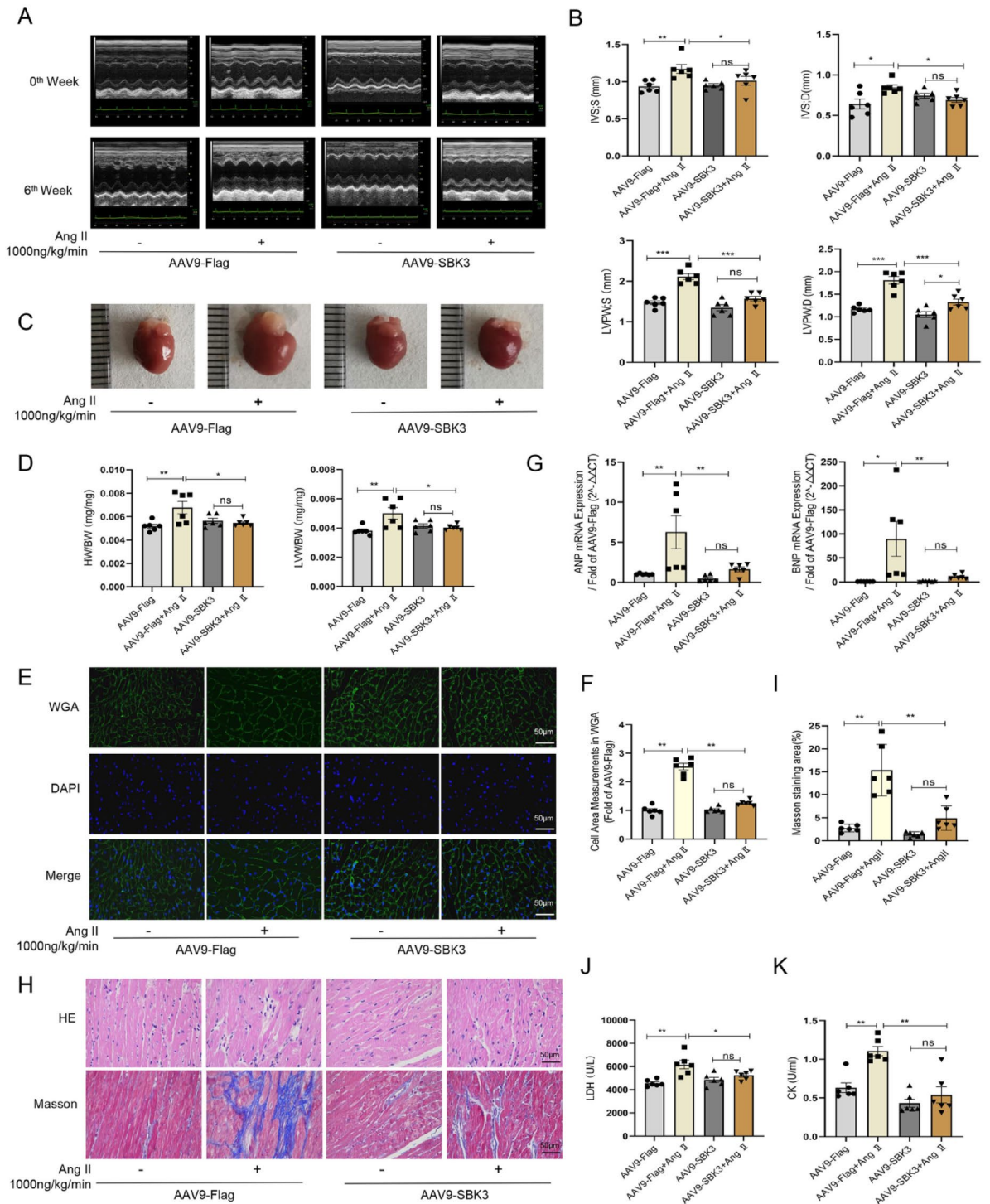


Fig. 3. Overexpression of SBK3 via the AAV9 vector suppressed Ang II-induced cardiac hypertrophy in mice. **(A, B)** AAV9-SBK3 decreased the left ventricular posterior wall thickness at systole (LVPW;S), left ventricular posterior wall thickness at diastole (LVPW;D), interventricular septal thickening at systole (IVS;S) and interventricular septal thickening at diastole (IVS;D) in mice induced by Ang II (1000 ng/kg/min), as determined by M-mode echocardiography. **(C)** Representative images of mouse heart in each group (scale bar = 1 mm), **(G–J)** AAV9-SBK3 reduced the HW/BW, LVWBW **(D)**, cross-sectional area of cardiomyocytes **(E and F)**, scale bar = 50 μm) and mRNA expression of ANP, BNP **(G)** altered by Ang II (1000 ng/kg/min) in mice. **(K–N)** The area of Masson’s trichrome **(H and I)**, scale bar = 50 μm) and the LDH **(J)**, CK **(K)** levels decreased after AAV9-SBK3 injection; n = 6 mice per group. The data were expressed as Mean ± SEM. **P* < 0.05, ***P* < 0.01, ****p* < 0.001, ns, non significant; one-way ANOVA test, followed by the Newman–Keuls test.

Overexpression of SBK3 in cardiac tissue effectively reduced the heart volume of mice with myocardial hypertrophy (Fig. 3C) and decreased the ratio of heart weight/body weight (HW/BW) and left ventricular weight/body weight (LVW/BW) (Fig. 3D). Additionally, wheat germ lectin (WGA) staining (Fig. 3E,F) demonstrated a significant reduction in the cross-sectional area of cardiomyocytes in mice with over-expressed SBK3. Notably, AAV9-SBK3 also led to a decrease in both ANP and BNP mRNA levels (Fig. 3G), which are typically elevated after exposure to Ang II. It was further confirmed *in vitro* that overexpression of SBK3 suppressed Ang II-induced hypertrophy in neonatal rat cardiomyocytes, evidenced by the reduced mRNA expression levels of ANP, BNP (Fig. S1C) and decreased cell size (Fig. S1D,E).

Furthermore, Ang II induced the disordered myocardial tissue architecture and a substantial increase in Masson's trichrome-stained areas (Fig. 3H,I), indicating the occurrence of myocardial injury and fibrosis after exposure to Ang II. We observed some minor fibrotic changes in the Masson-stained sections in some individual myocardium of mouse with overexpressed SBK3. While these findings were not statistically significant, they may be due to individual variations or potential reactions to elevated levels of SBK3 in otherwise healthy mice.

In addition, a significant increase in the levels of creatine kinase (CK) and lactate dehydrogenase (LDH) in the serum of mice following Ang II stimulation were observed (Fig. 3J,K). Notably, AAV9-SBK3 prominently reduced CK and LDH levels while restoring orderly myocardial arrangement with rich and uniform cytoplasm. The degree of Masson staining returned to normal. Collectively, these findings demonstrated that SBK3 overexpression effectively inhibited Ang II-induced myocardial hypertrophy and damage, including the attenuation of myocardial fibrosis *in vivo*. These results were consistent with our *in vitro* findings and supported the potential of SBK3 as a therapeutic target for cardiac hypertrophy.

AAV9-SBK3 mediates mitochondrial homeostasis in Ang II-perfused mice

The results of transmission electron microscopy revealed that treatment with Ang II resulted in a decrease in mitochondrial crista density and abundance, along with noticeable swelling and rupture of the mitochondria. Additionally, disruption of myofilaments and blurred sarcomeres were observed. However, overexpression of SBK3 restored crista integrity and arrangement, leading to improved mitochondrial morphology with an increased number of cristae. Overall, SBK3 overexpression improved the ultrastructure of mitochondria in mice subjected to Ang II perfusion (Fig. 4A).

Furthermore, Western blot analysis of the mitochondrial respiratory chain complexes in the heart (Fig. 4B,C) revealed that Ang II decreased the expression level of mitochondrial complex I and II in mice heart. However, overexpression of SBK3 in heart reversed this effect, restoring mitochondrial complex I and II expression levels.

Our findings demonstrated a significant decrease in the expression levels of Mitofusin-1 (Mfn1), Mitofusin-2 (Mfn2), and optic atrophy 1 (OPA1) following Ang II infusion (Fig. 4D,E). Additionally, we observed a reduction in overall protein levels of Dynamin-related protein 1 (Drp1) accompanied by an increase in phosphorylated Drp1 (p-Drp1) expression levels (Fig. 4F,G). These results indicated that Ang II disrupted mitochondrial dynamics in cardiac tissue. Importantly, overexpression of SBK3 effectively inhibited the phosphorylation of Drp1 at serine 616 (S616) while simultaneously restoring Mfn2 expression. In summary, our study highlighted the ability of SBK3 overexpression to maintain mitochondrial stability and inhibit Ang II-induced cardiac hypertrophy in mice.

Overexpression of SBK3 rebalances the level of the mitochondrial oxidative stress and energy metabolism in rat cardiomyocytes

To determine the subcellular localization of SBK3 in cardiomyocytes, we conducted Western blot and immunofluorescence analyses using subcellular organelles. The Western blot results revealed that the endogenous SBK3 protein bands were predominantly present in the mitochondrial group of adult rat cardiomyocytes, while they were not detected in the cytoplasmic group lacking mitochondria (Fig. 5A). We visualized the organelle localization of exogenous SBK3 through cellular immunofluorescence by transfecting adenovirus-overexpressing SBK3 in cardiomyocytes (Fig. 5B,C). We found that the red fluorescent part overlapped with the blue fluorescent part (Fig. 5D), showing the characteristic parallel arrangement between fasciculated myofilaments of adult rat cardiomyocytes. That is, the arrangement of SBK3 is completely consistent with that of mitochondria of cardiomyocytes, indicating that SBK3 is mainly located at mitochondria of cardiomyocytes. However, in addition to mitochondria, blue fluorescent spots were also observed in the nucleus, similar to the results of U2OS cells in the Protein database "the human protein atlas" (HPA, <https://www.proteinatlas.org/>). Combined with the results of Western blot (Fig. 5A), it was suggested that SBK3 was mainly located at the mitochondria of cardiomyocytes.

Our findings indicated that following Ang II (5 μ M, 24 h) stimulation, there was a significant increase in the levels of mitochondrial ROS (Fig. 5E) and malondialdehyde (MDA) (Fig. 5F), accompanied by a decrease in total SOD levels (Fig. 5G), suggesting heightened superoxide production and severe oxidative stress. Notably, Overexpression of SBK3 in cardiomyocytes significantly reduced mitochondrial ROS and malondialdehyde levels, indicating that SBK3 overexpression effectively mitigated the oxidative stress associated with Ang II-induced myocardial hypertrophy. However, no change was observed in the total levels of SOD. Therefore, we assessed the activity of mitochondrial SOD₂ (Fig. 5H). Our findings revealed a significant decrease in SOD₂ levels following the administration of Ang II. Conversely, overexpression of SBK3 completely reversed these changes by significantly enhancing the level of SOD₂. These results suggested that SBK3 effectively responded to oxidative stress in cardiomyocytes by increasing the mitochondrial abundance of SOD rather than its cytoplasmic content.

We conducted an investigation into the impact of SBK3 overexpression on oxygen consumption (OCR) and ATP levels in cardiomyocytes after Ang II stimulation. We observed a significant decrease in ATP production in ARCMs after administration of Ang II (Fig. 5I). The mitochondrial respiratory oxygen consumption rate (OCR) also decreased (Fig. 5J). Higher oxygen consumption rate (OCR) indicates higher electron transport

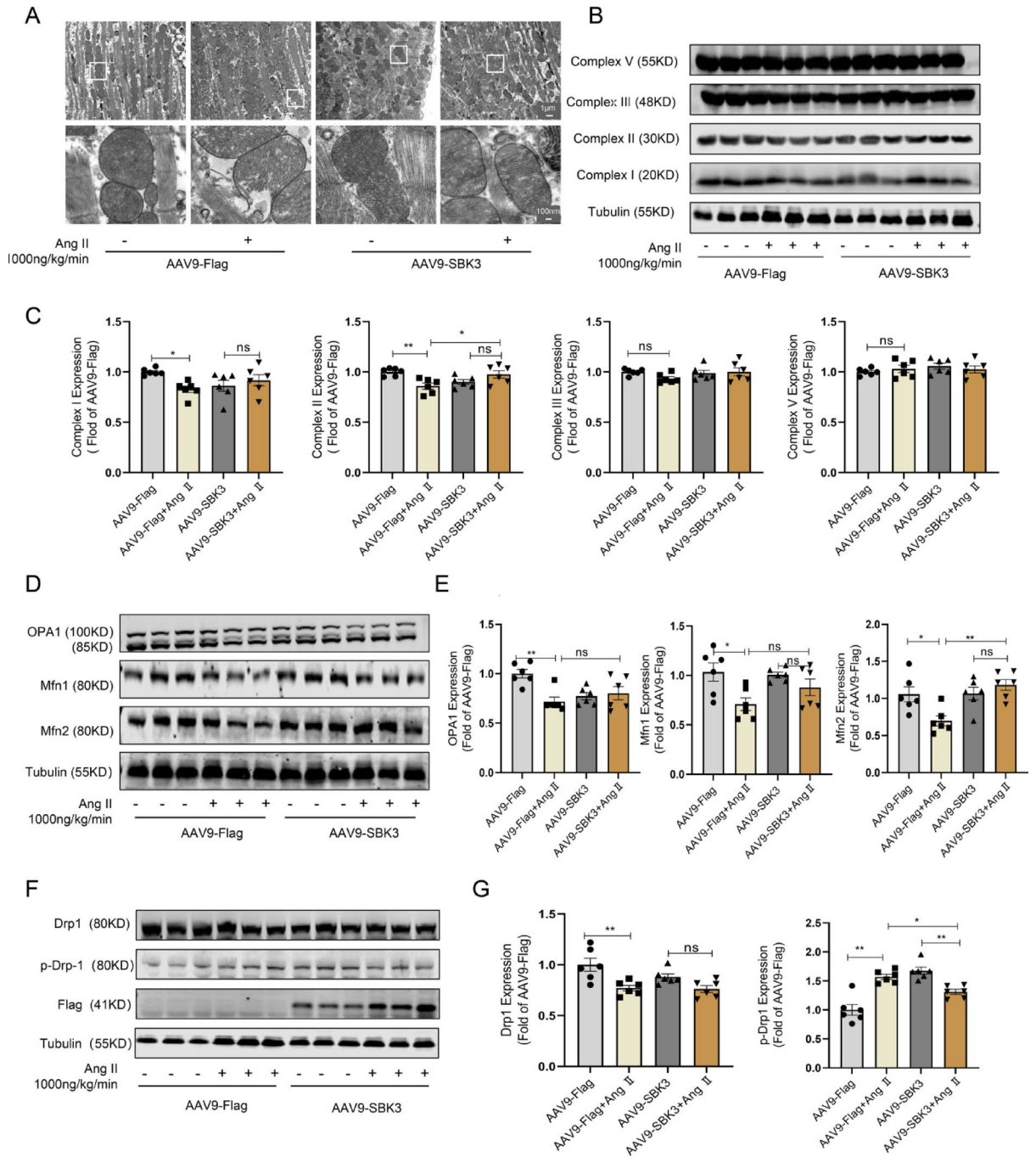


Fig. 4. AAV9-SBK3 was beneficial for maintaining the morphology and function of mitochondria after Ang II administration in mice. **(A)** Representative images of mitochondrial transmission electron microscopy in cardiac tissue of each mouse group, scale bar = 500 nm. **(B–G)** Mitochondrial respiratory chain complex I–V (**B**: representative images of western blot, **C**: quantitative analysis), OPA1, Mfn1, Mfn2 (**D**: representative images, **E**: quantitative analysis), Drp1, p-Drp1 (**F**: representative images, **G**: quantitative analysis) were rebalanced after SBK3 overexpression in mice. NADH-Q oxidoreductase (complex I), succinate-Q oxidoreductase (complex II), UQ-cytochrome C oxidoreductase (complex III), ATP synthetase (complex V). n = 6 mice per group. The data were expressed as Mean ± SEM. **P* < 0.05, ***P* < 0.01, ****p* < 0.001, ns, non significant; one-way ANOVA test followed by the Newman–Keuls test.

chain activity to meet cellular ATP requirements⁸. This may be the key for SBK3 to maintain energy metabolic homeostasis in cardiomyocytes in pathological states.

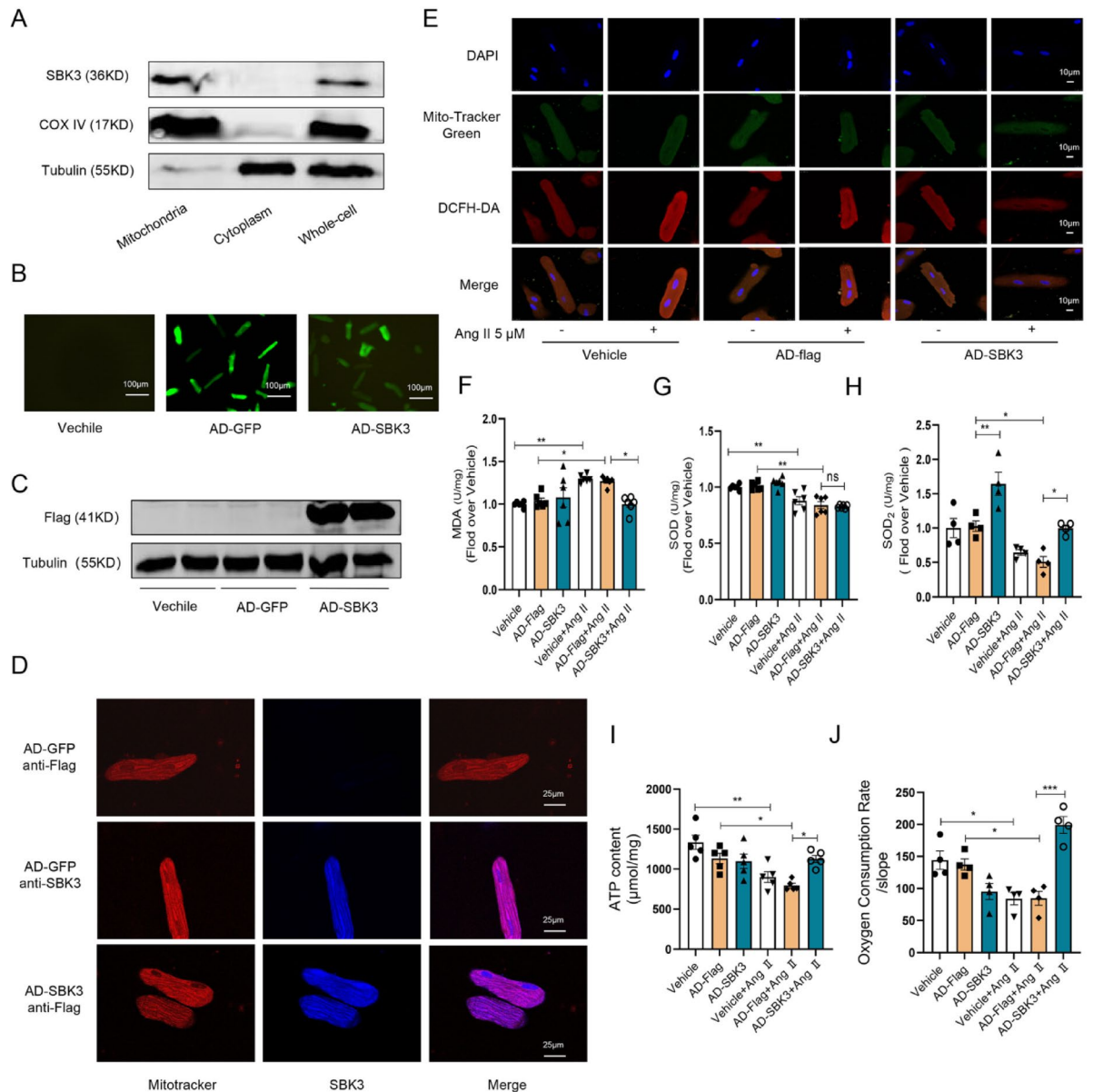


Fig. 5. The mitochondrial protein SBK3 rebalanced the level of oxidative stress and energy metabolism in cardiomyocytes induced by Ang II. **(A)** SBK3 was located in the mitochondria of rat cardiomyocytes, evidenced by Western blot, similar data in three experiment. **(B, C)** Verification of SBK3 overexpression in ARCMs based on **(B)**, scale bar = 100 μm) GFP fluorescence and **(C)** protein (western blot) expression **(D)** Representative images of SBK3 expression (anti-SBK3 or anti-Flag) co-localized with mitochondria, scale bar = 25 μm . **(E)** Overexpression of SBK3 restored the level of mitochondrial ROS induced by Ang II in ARCMs stained with DCFH-DA, as shown by confocal microscopy, scale bar = 10 μm . **(F–H)** Overexpression of SBK3 reduced the levels of MDA **(F)**, increased the level of SOD in mitochondria (SOD₂) **(H)**, but not in the cytoplasm (total SOD) **(G)**. **(I, J)** Overexpression of SBK3 enhanced the production of ATP **(I)** and the rate of oxygen consumption **(J)** in the ARCMs induced by Ang II (5 μM , 24 h). The data were expressed as Mean \pm SEM. * $P < 0.05$, ** $P < 0.01$, *** $P < 0.001$, ns, non significant; one-way ANOVA test, followed by the Newman–Keuls test.

Overexpression of SBK3 restores the expression of proteins related to mitochondrial dynamics induced by Ang II in rat cardiomyocytes

The Western blot technique was employed to evaluate the expression of mitochondrial fusion proteins and mitochondrial fission proteins in ARCMs. After 24 h of Ang II stimulation in cardiomyocytes, we observed a significant decrease in the levels of OPA1, Mfn1 and Mfn2 protein, which mediates mitochondrial fusion. Overexpression of SBK3 did not have any effect on the expression of OPA1 protein. However, overexpression of SBK3 in cardiomyocytes led to a significant upregulation in the expression of Mfn1 and partially restored the expression of Mfn2 (Fig. 6A,B).

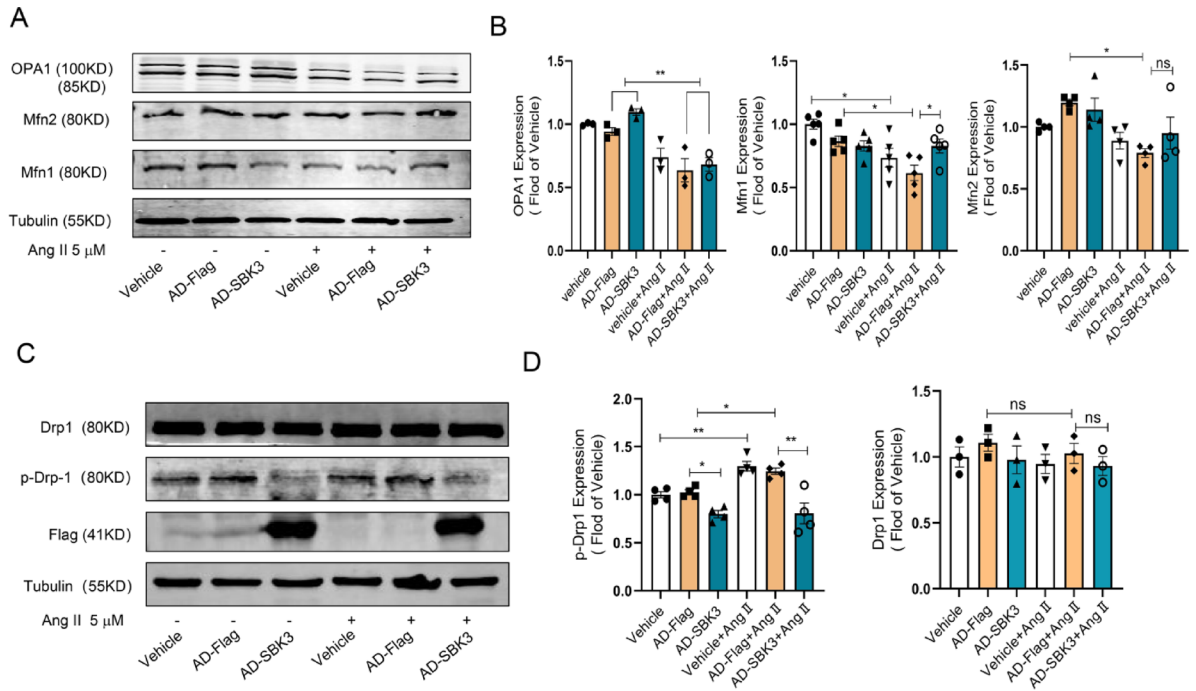


Fig. 6. Overexpression of SBK3 suppressed Drp1 phosphorylation at S616 in ARCMs. **(A,B)** Representative images **(A)** and quantitative analysis of OPA1 ($n = 3$), Mfn1 ($n = 5$), Mfn2 ($n = 4$) protein expression detected by western blot in rat cardiomyocytes after 5 μM of Ang II for 24 h **(B)**. **(C,D)** Representative images **(C)** and quantitative analysis of Drp1 ($n = 3$), p-Drp1 ($n = 4$) protein expression detected by western blot in rat cardiomyocytes after 5 μM of Ang II for 24 h **(D)**. Overexpression of SBK3 reduced the level of p-Drp1 in rat cardiomyocytes. The data were expressed as Mean \pm SEM. * $P < 0.05$, ** $P < 0.01$, ns, non significant; one-way ANOVA test, followed by the Newman–Keuls test.

As for a mitochondrial division, we found that there was an increase in p-Drp1 levels after Ang II administration, but total levels of Drp1 remained unchanged. This indicated that mitochondrial dynamics were tilted towards mitochondrial division at this time. Notably, overexpression of SBK3 significantly reversed p-Drp1 levels in Ang II-treated ARCMs (Fig. 6C,D). Furthermore, regardless of the presence or absence of Ang II, overexpression of SBK3 significantly reduced p-Drp1 levels. These results suggested a close relationship between SBK3-mediated anti-hypertrophy effects and regulation p-Drp1.

Discussion

Disruption of mitochondrial homeostasis is intricately closely related to the development of cardiac hypertrophy and subsequent heart failure^{25,26}. Studies have shown that cardiac hypertrophy inducers such as Ang II, α - and/or β -adrenergic receptor activation, as well as pressure/volume overload, can lead to mitochondrial dysfunction^{27,28}. It is first reported as we know that SBK3 is mainly located in the mitochondria in rat cardiomyocytes, which are the primary site of energy metabolism in the heart, an organ known for its high energy consumption. For functional consequence, present study has found a notable decrease in the expression of SBK3 protein in cases of cardiac hypertrophy in mice. Therefore, we hypothesize that SBK3 may serve as a highly promising therapeutic target for the prevention or treatment of cardiac hypertrophy by targeting mitochondria. We found that overexpression of SBK3 has been shown to suppress cardiac hypertrophy induced by Ang II in vitro and in vivo, suggesting that SBK3 could serve as a hypertrophy suppressor.

The anti-cardiac hypertrophic effect of SBK3 is attributed to its mitochondrial localization. It is well known that mitochondria possess their own genetic material, known as mitochondrial DNA (mtDNA), which is a 16.5 Kb closed-loop double-stranded DNA molecule²⁹. Mitochondria contain their own DNA, which encodes only 2 rRNAs, 22 tRNAs, and 13 proteins as respiratory chain subunits. Recently, using subcellular proteomic sequencing technology, approximately 4900 mitochondrial proteins were identified from the mouse heart proteome³⁰. In the purified mitochondria of mouse myocardium, 940 different proteins were identified, of which 480 were newly identified mitochondrial proteins³¹. Among these 940 proteins, only 59 were classified as “functionally unknown” proteins, including the SBK3 (SH3 domain binding kinase family member 3) protein. About 80% of the proteins in the 615 human heart mitochondrial proteome play a role in oxidative phosphorylation, RNA, DNA and protein synthesis, ion transport, and metabolism. However, the function of approximately 20% of human mitochondrial proteins, including SBK3, has not been confirmed or defined³². Other studies have shown that mitochondrial protein profiles undergo changes during ischemia–reperfusion injury. Therefore, further determination of the unknown mitochondrial proteome and its related protein

functions will help us understand the biological effects of mitochondria on myocardial morphology, function, and energy production under physiological and pathophysiological conditions.

Mitochondrial function is directly reliant on the integrity, transcription, and replication of mtDNA. In failing human hearts, there is a significant reduction in both mtDNA content and the expression of mtDNA-encoded proteins³³. Furthermore, it has been found that reactive oxygen species (ROS) produced by mitochondria are responsible for causing damage to mtDNA³⁴. Overexpression of SBK3 has been shown to reduce the production of reactive oxygen species (ROS) and the lipid peroxidation product malonaldehyde (MDA) in cardiomyocytes by increasing the content of the antioxidant enzyme SOD₂ in mitochondria in our data. On the other hand, during cardiac hypertrophy and heart failure, metabolic remodeling of the heart results in a decreased capacity for ATP production, leading to cardiomyocyte hypertrophy and cardiac dysfunction^{35,36}. However, overexpression of SBK3 significantly increased ATP production, improved the respiratory and oxygen consumption rate of cardiomyocytes, and ensured the energy metabolism demand of cardiomyocytes.

The anti-cardiac hypertrophy effect of SBK3 is also attributed to its capacity to regulate the expression of mitochondrial fission and fusion proteins, thereby maintaining a balance in mitochondrial dynamics. An increasing number of studies has demonstrated that enhancing mitochondrial fusion and reducing fission can prevent or reverse cardiac hypertrophy and improve cardiac function³⁷. Our findings indicate that the overexpression of SBK3 significantly inhibited the phosphorylation of Drp1 at S616 both in vitro and in vivo.

Increased mitochondrial fragmentation, decreased mitochondrial density, and increased apoptotic events have been observed in various forms of cardiomyopathy, including cardiac hypertrophy, ischemia/reperfusion (I/R), and heart failure³⁸. However, the proliferation of mitochondria in pathological states does not lead to improved ATP production³⁹. This is mainly due to the fact that the higher frequency of mitochondrial fusion-division accelerates the accumulation of mutated mtDNA^{40,41}. This eventually leads to severe ATP depletion. Mechanistically, this effect is mediated by the phosphorylation of Drp1 at the S616 site⁴². Inhibition of Drp1 activity blocked CaMKII-induced mPTP opening and cardiomyocyte death in vitro, and it prevented cardiac hypertrophy in vivo^{43,44}. Therefore, targeting mitochondrial Drp1 has become one of the ways to protect the heart. For example, the neuraminidase 1 inhibitor inhibits Drp1-dependent mitochondrial autophagy to protect against adriamycin-induced cardiotoxicity⁴⁵. Our data showed that Ang II increased the phosphorylation of Drp1 at S616. Overexpression of SBK3 significantly inhibited the phosphorylation of Drp1 at S616. To identify proteins associated with the effects of both SBK3 and Drp1, the present study employed co-immunoprecipitation techniques followed by mass spectrometry analysis, we found that a total of 151 of proteins were identified as forming immune complexes with SBK3, including 29 of mitochondrial proteins. Interestingly, following stimulation with AngII (5 μM), the number of proteins within the SBK3 immune complex was dropped to 90 (a reduction of 40%), while the count of mitochondrial proteins diminished to 9 (representing a decrease of 69%) (Fig. S 2). These findings suggest that SBK3 is closely associated with mitochondrial function and serves as a critical player in AngII-induced cardiac hypertrophy. Thus, it is worth to further study how SBK3 regulates Drp1 in structure and function. In addition, it is noted that there are slight fibrotic changes in myocardium of mice with overexpression of SBK3 although there is no statistically different in present study. The potential side effects of gene therapy warrant our careful consideration as well.

In conclusion, maintaining high expression of SBK3 represents a novel potential approach for the prevention or treatment of cardiac hypertrophy.

Data availability

Data are available from the corresponding author's upon reasonable request.

Received: 28 November 2024; Accepted: 3 June 2025

Published online: 02 July 2025

References

- Slivnick, J. & Lampert, B. C. Hypertension and heart failure. *Heart Fail. Clin.* **15**, 531–541. <https://doi.org/10.1016/j.hfc.2019.06.007> (2019).
- Sorrentino, M. J. The evolution from hypertension to heart failure. *Heart Fail. Clin.* **15**, 447–453. <https://doi.org/10.1016/j.hfc.2019.06.005> (2019).
- Sabbah, H. N. The cellular and physiologic effects of beta blockers in heart failure. *Clin. Cardiol.* **22**(Suppl 5), V16–20 (1999).
- Hartupee, J. & Mann, D. L. Neurohormonal activation in heart failure with reduced ejection fraction. *Nat. Rev. Cardiol.* **14**, 30–38. <https://doi.org/10.1038/nrcardio.2016.163> (2017).
- Kang, P. M. Novel pharmacological therapies for cardiac hypertrophy and heart failure. *Curr. Pharm. Des.* **17**, 1773. <https://doi.org/10.2174/138161211796390985> (2011).
- Dzudie, A. et al. Survival rate and predictors of 36-month mortality in patients with heart failure in Sub Saharan Africa: insights from the Douala Heart Failure Registry (Do-HF). *Cardiovasc. Diagn. Ther.* **12**, 577–588. <https://doi.org/10.21037/cdt-22-166> (2022).
- Manolis, A. S. et al. Mitochondrial dysfunction in cardiovascular disease: Current status of translational research/clinical and therapeutic implications. *Med. Res. Rev.* **41**, 275–313. <https://doi.org/10.1002/med.21732> (2021).
- Janz, A. et al. Mutations in DNAJC19 cause altered mitochondrial structure and increased mitochondrial respiration in human iPSC-derived cardiomyocytes. *Mol. Metab.* **79**, 101859. <https://doi.org/10.1016/j.molmet.2023.101859> (2024).
- Zhang, N. et al. HINT2 protects against pressure overload-induced cardiac remodeling through mitochondrial pathways. *J. Cell. Mol. Med.* **28**, e18276. <https://doi.org/10.1111/jcmm.18276> (2024).
- Xu, W. et al. Novel pan-ERR agonists ameliorate heart failure through enhancing cardiac fatty acid metabolism and mitochondrial function. *Circulation* **149**, 227–250. <https://doi.org/10.1161/CIRCULATIONAHA.123.066542> (2024).
- Miranda-Silva, D. et al. Mitochondrial reversible changes determine diastolic function adaptations during myocardial (reverse) remodeling. *Circ. Heart Fail.* **13**, e006170. <https://doi.org/10.1161/CIRCHEARTFAILURE.119.006170> (2020).
- Cao, Y. et al. Miro2 regulates inter-mitochondrial communication in the heart and protects against TAC-induced cardiac dysfunction. *Circ. Res.* **125**, 728–743. <https://doi.org/10.1161/CIRCRESAHA.119.315432> (2019).

13. Gibb, A. A. & Hill, B. G. Metabolic coordination of physiological and pathological cardiac remodeling. *Circ. Res.* **123**, 107–128. <https://doi.org/10.1161/CIRCRESAHA.118.312017> (2018).
14. Wetherill, L. et al. Genome-wide association study identifies loci associated with liability to alcohol and drug dependence that is associated with variability in reward-related ventral striatum activity in African- and European-Americans. *Genes Brain Behav.* **18**, e12580. <https://doi.org/10.1111/gbb.12580> (2019).
15. Wang, P., Guo, J., Wang, F., Shi, T. & Ma, D. Human SBK1 is dysregulated in multiple cancers and promotes survival of ovary cancer SK-OV-3 cells. *Mol. Biol. Rep.* **38**, 3551–3559. <https://doi.org/10.1007/s11033-010-0465-8> (2011).
16. Chen, X. et al. SH3 domain-binding kinase 1 promotes proliferation and inhibits apoptosis of cervical cancer via activating the Wnt/beta-catenin and Raf/ERK1/2 signaling pathways. *Mol. Carcinog.* **62**, 1147–1162. <https://doi.org/10.1002/mc.23552> (2023).
17. Guo, Q. et al. A novel risk model of three gefitinib-related genes FBP1, SBK1 and AURKA is related to the immune microenvironment and is predicting prognosis of lung adenocarcinoma patients. *Aging (Albany NY)* **15**, 9633–9660. <https://doi.org/10.18632/aging.205040> (2023).
18. Hu, Z. W. et al. CD69 and SBK1 as potential predictors of responses to PD-1/PD-L1 blockade cancer immunotherapy in lung cancer and melanoma. *Front. Immunol.* **13**, 952059. <https://doi.org/10.3389/fimmu.2022.952059> (2022).
19. van Gorp, P. R. R. et al. Sbk2, a newly discovered atrium-enriched regulator of sarcomere integrity. *Circ. Res.* **131**, 24–41. <https://doi.org/10.1161/CIRCRESAHA.121.319300> (2022).
20. Ma, E. et al. Resveratrol prevents Ang II-induced cardiac hypertrophy by inhibition of NF-kappaB signaling. *Biomed. Pharmacother.* **165**, 115275. <https://doi.org/10.1016/j.biopha.2023.115275> (2023).
21. Guo, B. et al. Cardiac protection of a novel Lupane-type triterpenoid from injuries induced by hypoxia-reperfusion. *Int. J. Mol. Sci.* **23**, 9473. <https://doi.org/10.3390/ijms23169473> (2022).
22. Wang, J. et al. Phenylephrine promotes cardiac fibroblast proliferation through calcineurin-NFAT pathway. *Front. Biosci. (Landmark Ed.)* **21**, 502–513. <https://doi.org/10.2741/4405> (2016).
23. Zhao, L. L. et al. HSC70-JNK-BAG3 complex is critical for cardiomyocyte protection of BAG3 through its PXXP and BAG structural domains. *Front. Biosci. (Landmark Ed.)* **26**, 102–113. <https://doi.org/10.52586/4927> (2021).
24. Yao, N. et al. beta-arrestin2 mediates the arginine vasopressin-induced expression of IL-1beta in murine hearts. *Front. Biosci. (Landmark Ed.)* **28**, 7. <https://doi.org/10.31083/j.fb12801007> (2023).
25. Lv, L. et al. The lncRNA Plscr4 controls cardiac hypertrophy by regulating miR-214. *Mol. Ther. Nucleic Acids* **10**, 387–397. <https://doi.org/10.1016/j.omtn.2017.12.018> (2018).
26. Zhang, X. et al. Bawei Chenxiang Wan ameliorates cardiac hypertrophy by activating AMPK/PPAR-alpha signaling pathway improving energy metabolism. *Front. Pharmacol.* **12**, 653901. <https://doi.org/10.3389/fphar.2021.653901> (2021).
27. Osterholt, M., Nguyen, T. D., Schwarzer, M. & Doenst, T. Alterations in mitochondrial function in cardiac hypertrophy and heart failure. *Heart Fail. Rev.* **18**, 645–656. <https://doi.org/10.1007/s10741-012-9346-7> (2013).
28. Nakamura, M. & Sadoshima, J. Mechanisms of physiological and pathological cardiac hypertrophy. *Nat. Rev. Cardiol.* **15**, 387–407. <https://doi.org/10.1038/s41569-018-0007-y> (2018).
29. Rosca, M. G., Tandler, B. & Hoppel, C. L. Mitochondria in cardiac hypertrophy and heart failure. *J. Mol. Cell. Cardiol.* **55**, 31–41. <https://doi.org/10.1016/j.yjmcc.2012.09.002> (2013).
30. Bousette, N. et al. Large-scale characterization and analysis of the murine cardiac proteome. *J. Proteome Res.* **8**, 1887–1901. <https://doi.org/10.1021/pr800845a> (2009).
31. Zhang, J. et al. Systematic characterization of the murine mitochondrial proteome using functionally validated cardiac mitochondria. *Proteomics* **8**, 1564–1575. <https://doi.org/10.1002/pmic.200700851> (2008).
32. Taylor, S. W. et al. Characterization of the human heart mitochondrial proteome. *Nat. Biotechnol.* **21**, 281–286. <https://doi.org/10.1038/nbt793> (2003).
33. Karamanlidis, G. et al. Defective DNA replication impairs mitochondrial biogenesis in human failing hearts. *Circ. Res.* **106**, 1541–1548. <https://doi.org/10.1161/CIRCRESAHA.109.212753> (2010).
34. Dai, D. F. et al. Mitochondrial oxidative stress mediates angiotensin II-induced cardiac hypertrophy and Galphaq overexpression-induced heart failure. *Circ. Res.* **108**, 837–846. <https://doi.org/10.1161/CIRCRESAHA.110.232306> (2011).
35. Dormann, N. et al. Metabolic remodeling in cardiac hypertrophy and heart failure with reduced ejection fraction occurs independent of transcription factor EB in mice. *Front. Cardiovasc. Med.* **10**, 1323760. <https://doi.org/10.3389/fcvm.2023.1323760> (2023).
36. Lopaschuk, G. D., Karwi, Q. G., Tian, R., Wende, A. R. & Abel, E. D. Cardiac energy metabolism in heart failure. *Circ. Res.* **128**, 1487–1513. <https://doi.org/10.1161/CIRCRESAHA.121.318241> (2021).
37. Yao, B. F., Luo, X. J. & Peng, J. A review for the correlation between optic atrophy 1-dependent mitochondrial fusion and cardiovascular disorders. *Int. J. Biol. Macromol.* **254**, 127910. <https://doi.org/10.1016/j.ijbiomac.2023.127910> (2024).
38. Sebastiani, M. et al. Induction of mitochondrial biogenesis is a maladaptive mechanism in mitochondrial cardiomyopathies. *J. Am. Coll. Cardiol.* **50**, 1362–1369. <https://doi.org/10.1016/j.jacc.2007.06.035> (2007).
39. Hansson, A. et al. A switch in metabolism precedes increased mitochondrial biogenesis in respiratory chain-deficient mouse hearts. *Proc. Natl. Acad. Sci. U. S. A.* **101**, 3136–3141. <https://doi.org/10.1073/pnas.0308710100> (2004).
40. Tam, Z. Y., Gruber, J., Halliwell, B. & Gunawan, R. Context-dependent role of mitochondrial fusion-fission in clonal expansion of mtDNA mutations. *PLoS Comput. Biol.* **11**, e1004183. <https://doi.org/10.1371/journal.pcbi.1004183> (2015).
41. Tam, Z. Y., Gruber, J., Halliwell, B. & Gunawan, R. Mathematical modeling of the role of mitochondrial fusion and fission in mitochondrial DNA maintenance. *PLoS ONE* **8**, e76230. <https://doi.org/10.1371/journal.pone.0076230> (2013).
42. Aung, L. H. H., Jumbo, J. C. C., Wang, Y. & Li, P. Therapeutic potential and recent advances on targeting mitochondrial dynamics in cardiac hypertrophy: A concise review. *Mol. Ther. Nucleic Acids* **25**, 416–443. <https://doi.org/10.1016/j.omtn.2021.06.006> (2021).
43. Xu, S. et al. CaMKII induces permeability transition through Drp1 phosphorylation during chronic beta-AR stimulation. *Nat. Commun.* **7**, 13189. <https://doi.org/10.1038/ncomms13189> (2016).
44. Jiang, W. et al. Hirsutine ameliorates myocardial ischemia-reperfusion injury through improving mitochondrial function via CaMKII pathway. *Clin. Exp. Hypertens.* **45**, 2192444. <https://doi.org/10.1080/10641963.2023.2192444> (2023).
45. Qin, Y. et al. Neuraminidase1 inhibitor protects against doxorubicin-induced cardiotoxicity via suppressing Drp1-dependent mitophagy. *Front. Cell. Dev. Biol.* **9**, 802502. <https://doi.org/10.3389/fcell.2021.802502> (2021).

Acknowledgements

This work was supported by the National Natural Science Foundation of China (Grant No.81770400).

Author contributions

Conceptualization: W.-Z.Z.; Designed the study and the experiments: W.-Z.Z., A.-H.Y., J.-X.C., J.-N.G.; Methodology: W.-Z.Z., A.-H.Y., J.-X.C., J.-N.G, X.-F.Z., Y.Q., H.-Y.Q., W.-J.Z., Y.-H.W.; Analyzed the data: A.-H.Y., J.-X.C., J.-N.G, Y.Q., W.-J.Z., Y.-H.W.; Prepared the figures: A.-H.Y., J.-X.C., J.-N.G; Wrote the first draft of the manuscript: A.-H.Y., J.-X.C., J.-N.G; Edited and finalized manuscript: W.-Z.Z., A.-H.Y. All authors reviewed the manuscript.

Declarations

Competing interests

The authors declare no competing interests.

Additional information

Supplementary Information The online version contains supplementary material available at <https://doi.org/10.1038/s41598-025-05584-y>.

Correspondence and requests for materials should be addressed to W.Z.

Reprints and permissions information is available at www.nature.com/reprints.

Publisher's note Springer Nature remains neutral with regard to jurisdictional claims in published maps and institutional affiliations.

Open Access This article is licensed under a Creative Commons Attribution-NonCommercial-NoDerivatives 4.0 International License, which permits any non-commercial use, sharing, distribution and reproduction in any medium or format, as long as you give appropriate credit to the original author(s) and the source, provide a link to the Creative Commons licence, and indicate if you modified the licensed material. You do not have permission under this licence to share adapted material derived from this article or parts of it. The images or other third party material in this article are included in the article's Creative Commons licence, unless indicated otherwise in a credit line to the material. If material is not included in the article's Creative Commons licence and your intended use is not permitted by statutory regulation or exceeds the permitted use, you will need to obtain permission directly from the copyright holder. To view a copy of this licence, visit <http://creativecommons.org/licenses/by-nc-nd/4.0/>.

© The Author(s) 2025